中國機械工程學會第十一屆全國學術研討會

固體力學組　論文集

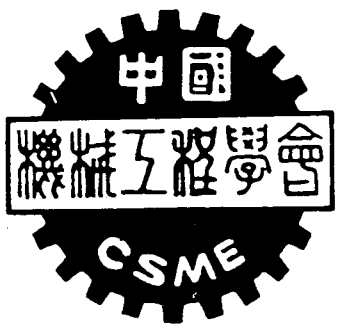

PROCEEDINGS OF THE ELEVENTH NATIONAL
CONFERENCE OF THE CHINESE SOCIETY OF
MECHANICAL ENGINEERS

TAICHUNG, TAIWAN
REPUBLIC OF CHINA
NOVEMBER, 1994

台中市　國立中興大學
中華民國八十三年十一月

OPTIMAL PLACEMENT OF PIEZOELECTRIC TRANSDUCERS IN ACTIVE STRUCTURAL ACOUSTIC CONTROL

BOR-TSUEN WANG

Department of Mechanical Engineering
National Pingtung Polytechnic Institute
Pingtung, Taiwan 91207

ABSTRACT

This paper presents an optimum design methodology for positioning PZT actuators and PVDF sensors in active structural acoustic control. A simply-supported beam in an infinite rigid baffle subject to a harmonically excited point force is considered. The piezoceramic patches are adhered to the beam acting as control transducers, while PVDF films are used as structural error sensors with the adoption of LMS feedforward Control. The optimization problem is formulated by constructing the objective function based on the total radiated sound power and identifying the design variables which are the locations of PZT actuators and PVDF sensors. The genetic algorithm (GA) incorporated with the use of linear quadratic optimal control theory (LQOCT) to calculate the control voltages to the actuators is adopted to determine the optimal locations of finite size PZT actuators and PVDF sensors. The GA is shown a suitable mean for determining the optimal placement of actuators and sensors. Results show that the optimal placed PZT actuators and PVDF sensors can perform better sound radiation control than the arbitrarily selected ones. In particular, for off-resonance excitation cases the optimized PZT actuators and PVDF sensors can efficiently control the sound radiation and eliminate the spillover. Radiation directivity patterns and beam displacement distributions are shown to demonstrate the control mechanisms of piezoceramic transducers as well as a wavenumber analysis.

INTRODUCTION

Piezoceramic materials such as PZT and polyvinylidene fluoride (PVDF) have been widely adopted as control transducers for active structural acoustic control. PZT actuation dynamic models for various structures have been developed and can provide the fundamental base of theoretical analysis for their implementation in structural vibration or sound radiation control [1-5]. Experiments have also been conducted to verify the application of PZT actuation models for dynamic excitation of the structures [6-8]. Previous works showed that PZT can be potentially used as actuators to actively control the structural vibration [1,9] as well as sound radiation/transmission from structures [7,8,10,11]. PVDF can serve as error sensors for vibration control [9,12]. Recently, PVDF have also been applied to sound radiation control serving as near-field structural sensors and can achieve sufficient control performance [13,14].

The tailoring of actuators and sensors are very important in terms of control performance. While researches focus on the development of actuation and sensing techniques, the optimization of the placement of actuators and sensors are also a great deal of interest. The optimal placement of actuators and sensors have been extensively studied [15-18]. However, most of those works considered the conventional transducers such as shakers, accelerometers and microphones. Upon the popular use of piezoceramic transducers, their optimal location is also a great deal of concern [19-22]. Previous works [21,22] developed a nonlinear optimization technique to optimally locate the PZT actuators and PVDF sensors for plate sound radiation control. The optimal solution is obtained by a traditional gradient search method which requires extensive computing efforts. Since the objective function to be minimized is a multi-minimum nonlinear function, seleHxing the initial guess can be critical to the optimal solution. In addition, another drawback of the gradient search method is its complexity for computer implementation. The genetic algorithm (GA) a simple algebraic calculation procedure based on the Darwin's theory of survival of the fittest has been widely applied to various types of optimization problems [23-25]. The GA can be easily programmed to determine the optimal location of actuators and sensors [26,27].

This paper considers a simply-supported beam mounted in an infinite rigid baffle subjected to a harmonic point force disturbance. While PVDF films are used as error sensors, the piezoceramic patches are implemented as control actuators in conjunction with the use of LMS feedforward control. A solution strategy

adopting the GA in conjunction with the use of linear quadratic optimal control theory (LQOCT) is proposed to determine the optimal location of PZT actuators and PVDF sensors. Both on- and off-resonance excitation cases are presented to demonstrate the control mechanism and performance of piezoceramic transducers. Results show that the optimally placed PZT actuators and PVDF sensors perform much better sound radiation control than the arbitrarily chosen. In particular, for off-resonance excitation the optimally positioned actuators and sensors can significantly achieve efficient sound radiation control in comparison with the arbitrarily selected ones. This work provides an optimum design methodology for positioning actuators and sensors in active structural acoustic control.

SOUND RADIATION FROM THE BEAM

The sound pressure radiated to the far-field from a simply-supported beam in an infinite rigid baffle, as shown in Figure 1, can be derived from the Rayleigh integral as follow [28]:

$$p(r,\theta,\phi,t)=e^{i\omega t}\sum_{n=1}^{\infty} W_n q_n \tag{1}$$

where

$$W_n=\frac{P_n}{\rho_b b t_b(\omega_n^2-\omega^2)} \tag{2}$$

$$q_n=-i\omega\frac{\rho c b}{\pi}\frac{\kappa}{\alpha_n}\frac{e^{-i\kappa r}}{2r}\left[\frac{1-(-1)^n e^{-i\alpha}}{1+(\alpha/n\pi)^2}\right]\left[\frac{1-e^{-i\beta}}{\beta}\right] \tag{3}$$

$$\omega_n=(n\pi)^2\sqrt{\frac{E_b I}{\rho_b b t_b L^4}} \tag{4}$$

$$\alpha_n=\frac{n\pi}{L} \tag{5}$$

$$\alpha=\kappa L\sin\theta\cos\phi \tag{6}$$

$$\beta=\kappa b\sin\theta\sin\phi \tag{7}$$

Here E_b is the Young's modulus of the beam; I the moment of inertia; ρ_b the beam density; t_b beam thickness; b beam width; ρ the air density; c the sound speed in air; κ the acoustic wavenumber; and P_n the modal force depending on the form of excitation. For a harmonic point force with the amplitude of F located at x_f acting on the beam, the modal force, P_n^f, is given as follow:

$$P_n^f=\frac{2F}{L}\sin\alpha_n x_f \tag{8}$$

For an actuator consisting of two identical piezoceramic patches bonded symmetrically on the two opposite beam surfaces and activated 180° out-of-phase, the equivalent external forces are the concentrated moments acting on the both edges of piezoceramic patches. The corresponding expression of modal force for piezoelectric excitation, P_n^c, can be derived [4] as follow:

$$P_n^c=\frac{2M_{eq}}{L}\alpha_n(\cos\alpha_n x_1-\cos\alpha_n x_2) \tag{9}$$

where x_1 and x_2 are the coordinates of the piezoelectric actuator; and M_{eq} is the resultant external moment due to the free piezoelectric strain induced by a voltage input.

Under the assumption of superposition, the total radiated sound pressure can be the sum of sound pressures due to the disturbance and control inputs

$$p_t=p_f+p_c=e^{i\omega t}\sum_{n=1}^{\infty}(W_n^f+W_n^c)q_n \tag{10}$$

The total radiated sound power defined as the integral of the square of the radiated sound pressure over the hemisphere of the radiating field can then be obtained:

$$\Phi_p=\frac{1}{2\rho c}\int_S |p_t|^2 dS=\frac{r^2}{2\rho c}\int_0^{2\pi}\int_0^{\pi/2}|p_t|^2\sin\theta d\theta d\phi \tag{11}$$

The total radiated sound power can be an index to evaluate the effectiveness of sound radiation control and can be chosen as the objective function for the purpose of optimization.

PVDF SENSOR'S EQUATION

For a PVDF film arranged as shown in Figure 1, the sensor's equation can then be derived as follows [9]:

$$V(t)=\frac{q(t)}{\epsilon A}t_s \tag{12}$$

where

$$q(t)=e^{i\omega t}\left(\frac{t_b+t_s}{2}e_{31}b_s\right)\sum_{n=1}^{\infty}\alpha_n W_n(\cos\alpha_n x_{s2}-\cos\alpha_n x_{s1}) \tag{13}$$

Here b_s is the sensor width; t_s the sensor thickness; e_{31} the piezoelectric field intensity constant; ϵ is the permittivity of PVDF films; A is the sensor area; x_{s1} and x_{s2} are the coordinates of the PVDF film. It is noted that the generated voltage is proportional to the slope difference between the two edges of a PVDF film.

WAVENUMBER ANALYSIS

The beam velocity transform can be obtained

by performing Fourier integral transform and can be expressed as [14]:

$$\tilde{V}(\kappa_x,\kappa_y)=i\omega\sum_{n=1}^{\infty} W_n V_n \tag{14}$$

where

$$V_n=i\alpha_n\left[\frac{1-(-1)^n e^{-i\kappa_x L}}{\alpha_n^2-\kappa_x^2}\right]\left[\frac{e^{-i\kappa_y b}-1}{\kappa_y}\right] \tag{15}$$

$$\kappa_x=\kappa\sin\theta\cos\phi \tag{16}$$

$$\kappa_y=\kappa\sin\theta\sin\phi \tag{17}$$

It is noted that the least mean square (LMS) value of the velocity transform, i.e., $|\tilde{V}|^2$, is proportional to the radiated sound power [29]. Only the wavenumber components satisfying $\kappa_x^2+\kappa_y^2<\kappa^2$ contribute to sound radiation into the far-field and are termed as supersonic waves. Other wavenumber components do not radiate into the far-field and are termed subsonic waves.

LINEAR QUADRATIC OPTIMAL CONTROL THEORY

For sound radiation control, microphones located in the far-field are generally used as error sensors; however, near-field structural sensors are preferred for easy implementation. The PVDF film, a distributed type of sensor, is recently applied to measure the structural response and acts as a near-field structural sensor to perform active sound radiation control. For the use of N_s PVDF sensors, the cost function can be defined as the sum of the mean square voltages measured from the PVDF films:

$$\Psi_v=\sum_{j=1}^{N_s}|V_j|^2 \tag{18}$$

The linear quadratic optimal control theory (LQOCT) can then be applied to minimize the cost function so as to find the optimal control voltages input to the piezoelectric actuators. The full analysis can be referred to [30] and omitted here for brevity.

GENETIC ALGORITHM

The genetic algorithm is derived based on Darwin's theory of "Survival of the Fittest" [23]. The GA is a search procedure for general optimization problems and is numerically simple involving nothing more than random number generation, bit manipulation and string exchange. The objective function is usually transformed to a fitness function

$$F(x)= \textit{base value} - f(x) \tag{19}$$

The GA is to maximize the fitness function, $F(x)$, in contrast to minimize the objective function, $f(x)$, in comparison with the traditional optimization procedures. The design variables, x, are encoded as a binary digit string which is analogous to chromosome in a biological system. When multiple design variables are desired, all design variables are concatenated to one single string. In the begin with, the GA randomly generates a population of strings by successive coin flips. The generation process is then succeeded to produce the new generation of population by performing three basic operators of GA: reproduction, crossover, and mutation. Strings can be decoded to obtain the exact values of the design variables in order to calculate the fitness values. The design constraints can be treated by the exterior penalty function method such that a constrained problem is transformed to an unconstrained problem.

FORMULATION OF OPTIMIZATION PROBLEM

As shown in Figure 1, a simply-supported beam in an infinite rigid baffle is considered as the plant subjected to a harmonically excited point force disturbance. The sound radiation from the beam is controlled by PZT actuators in conjunction with the use of LMS feedforward control algorithm, while PVDF sensors are used as error sensors. The size of the i-th PZT actuator and PVDF sensor is assumed to be fixed. The applied voltages to the piezoelectric actuators can be calculated from linear quadratic optimal control theory (LQOCT). Therefore, the design variables can be identified as:

$$\bar{x}_1,\bar{x}_2,\ldots,\bar{x}_{N_c},\tilde{x}_1,\tilde{x}_2,\ldots,\tilde{x}_{N_s} \tag{20}$$

where $\bar{x}_i$ and $\tilde{x}_i$ are the central location of the i-th PZT actuator and PVDF sensor respectively as illustrated in Figure 1. The objective function can then be defined as the total radiated power as shown in Equation (11) and transformed to a fitness function. Therefore, the genetic algorithm can then be applied to solve for the optimal locations of PZT actuators and PVDF sensors. The solution strategy is described as follow.

SOLUTION STRATEGY

The GA is implemented as FORTRAN codes incorporated with the use of LQOCT to calculate the optimal control voltages input to actuators whenever the location of actuators is determined. The solution flow chart is shown in Figure 2. The detail procedure is described as follow:

1. Setup GA constants. At the beginning of the program, some GA constants including population size for each generation, the string length of design variables, crossover probability, mutation probability and the number of maximum generation must be specified.

2. Generate initial population. The binary digit string is generated by successive coin flips. The design variables are encoded as a binary digit string. All design variables are concatenated to one single string.
3. Calculate the population statistics. In this stage, each string is decoded to obtain the exact values of design variables, which are the central location of PZT actuators and PVDF sensors. The LQOCT is then applied to calculate the control voltages input to the PZT actuators such that the fitness value can be computed. Finally, the maximum, averaged, minimum and sum of the fitness for the current generation can be obtained. Those values are required in the production of new generation.
4. Produce new generation. To produce a new generation, three basic GA operators, i.e., reproduction, crossover and mutation, are performed. A pair of reproduction mates are first selected by a roulette wheel with slots sized according to the fitness values. The crossover is then performed for the selected reproduction mates based on the crossover probability. Finally, the mutation is performed on the children sets to produce the new generation array.
5. Calculate the population statistics. The procedures are the same as those in Step 3.
6. Report results. This stage is to print out the results of population statistics as well as the string digit and the exact values of design variables for further analysis.
7. Repeat Steps 4 to 6 until the program reaches the number of maximum generation.

DESIGN PROCESSES

To determine the optimal locations of PZT actuators and PVDF sensors, three design processes are taken. First, the locations of PVDF sensors are assumed to be fixed, only the locations of PZT actuators are to be optimized. Second, when the optimal locations of the PZT actuators are obtained from design process I and assumed to be fixed, the locations of PVDF sensors are then optimized. Third, both the locations of PZT actuators and PVDF sensors are considered as design variables and determined simultaneously. Design processes I and II involve less design variables and thus require less computing effort than design process III. Design process III can simultaneously optimize the locations of actuators and sensors; however, more design variables will result in a larger solution domain. In the following numerical examples, each design variable is encoded by a ten digit string, which consists of $2^{10}=1024$ combinations of solutions. If two design variables are considered, the solution domain will be doubled. The GA thus may require more population sizes or generations to achieve the optimum or the maximum of the fitness. These design processes will be evaluated in the following numerical analysis.

ANALYTICAL RESULTS

A steel beam with length of 0.38 m, width of 0.04 m, and thickness of 2 mm is used in the simulations. Table I shows the natural frequencies of the simply-supported beam. It is noted that no damping was included in the following analysis. A harmonic point force with input parameters, $F=0.3$ N and $x_f=0.067$ m, was considered for the following analysis. The physical properties of the piezoelectric patch (G-1195) [31] and PVDF films (LDT-28 μ k) [32] are respectively shown in Tables II and III. The length of PZT actuators and PVDF sensors is assumed to be 0.0635 m and 0.04 m respectively. For design process I, the PVDF film is assumed to be located at $x_{s_1}=0.10$ m, $x_{s_2}=0.14$ m. For the purpose of comparison, an arbitrary set of PZT actuator and PVDF sensor is chosen. The piezoceramic patch is located at $x_1=0.285$ m, $x_2=0.3485$ m, and the PVDF film is located at $x_{s1}=0.10$ m, $x_{s2}=0.14$ m. In order to calculate the beam response and radiated sound pressure, it was necessary to truncate the modal sums in Equation (1). Upon consideration of computing time and accuracy, the first 10 modes were considered, and it was found to provide sufficient convergence of series.

Both the radiation directivity and beam displacement distributions were shown to demonstrate the control mechanisms of sound radiation from the beam. The radiated sound pressure is plotted in dB *re* 20×10^{-6} Pa over $\theta=-90°$ to $90°$ at a radial distance of 3 m from the beam, which is well into the far-field. The beam displacement distribution is normalized by the largest amplitude in each case and plotted in dB along the beam length.

In order to perform the genetic algorithm, the initial population size is assumed to be 20 for one design variable, 40 for two design variables, etc. The number of maximum generation is set to be 10. It is obvious that the solution time for two design variables will be twice of that for one design variable. The crossover and mutation probabilities are set to be 0.6 and 0.02 respectively. Each design variable is coded as a ten digit string such that the location accuracy is about 0.4 mm.

OPTIMAL LOCATION OF PZT ACTUATORS AND PVDF SENSORS

For design process I, the PVDF sensor is assumed to be fixed and located at $x_{s1}=0.10$ m, $x_{s2}=0.14$ m. A finite length of 0.0635 m PZT actuator is considered.

The location of one PZT actuator is to be optimized. The optimal locations of the PZT actuators for various excitation frequencies are listed in Table IV denoted by Design I. The bolded values indicates the on-resonance excitation cases. The optimal location of PZT actuator is dependent on the excitation frequency due to the variation of the modal transfer function in frequencies. The positions of the PZT actuator and PVDF sensor are depicted in Figure 3, and the associate vibration mode shapes are also plotted. For 33 Hz excitation case, i.e., near the first resonance mode, one edge of the PZT actuator is near the maximum response of the first mode shape. For 129 Hz excitation case, i.e., near the second resonance, one edge of the PZT actuator is close to the nodal point of the associated structural mode shape. For the third mode excitation, i.e., f=290 Hz, the PZT actuator is found to be about symmetrically located in a lobe of the mode shape. For off-resonance excitation cases, the edges of PZT actuators can also be found to be near the nodal point of the adjacent mode shapes. From the above observations, it is noted that the possible candidates of optimal locations of PZT actuators can be where their edges near the maximum response or the nodal point of the associated structural mode shapes and where the PZT actuators symmetrically distribute over a whole lobe of the associated mode shapes. For simple structures like one dimensional beam, these statements can be sufficiently true as discussed by Dimitriadis et al. [3] and Jia [19]. Dimitriadis et al. [3] claimed that the optimum boundary of the PZT actuator may be along the nodal lines of the associated mode shapes. Jia [19] showed that to maximize the length of the PZT actuator covering a whole lobe can effectively suppress the single mode response of beam vibration. However, for two dimensional structures like plates, structure/acoustic interaction is more complex involving two dimensional modal responses. As such situations, Wang et al. [21] showed that the PZT optimal location can be determined under a compromise to eliminate the several significant radiation modes. Therefore, the location of PZT actuators may not be intuitively derived. Table V shows the reduction of modal amplitudes, W_n, of the first five modes for design process I. The "-" negative values indicate the increase of modal amplitudes. One can observe that a significant amount of modal amplitudes have been eliminated near the excitation frequency, while this results in spillover to higher modes.

When the optimal location of the PZT actuator is obtained in design process I and assumed to be fixed, the optimal location of the PVDF sensor is then to be determined. The coordinates of the optimal PVDF sensors for various excitation frequencies are listed in Table IV and depicted in Figure 3 denoted by Design II. The PVDF sensors can be found to be located near the nodal point or the maximum response of the associated structural mode shape. It is noted that the PVDF sensor, in fact, measures the slope difference between the edges of the PVDF film. Therefore, the optimal location of PZT actuator is determined to minimize the maximum slope in the beam such that the sound radiation will be minimum. If the optimal locations of PZT actuators and PVDF sensors are to be determined simultaneously, i.e., design process III is adopted, their optimal locations are slightly different from design processes I and II. However, the PZT actuators and PVDF sensors are still located near those positions as discussed above.

EVALUATION OF DESIGN PROCESSES

Table VI shows the reduction of the total radiated sound power, Φ_p, which is selected as the objective function for optimization and can be an index to evaluate the effectiveness of sound radiation control. An arbitrary set of PZT actuator and PVDF sensor has been used in previous studied [14], and is selected for comparison. Either design processes I, II or III performs better sound radiation control than the arbitrary ones. In particular, for off-resonance excitation cases, the optimum design cases can significantly eliminate the sound radiation and reduce the spillover found in the arbitrary case. In addition, a large amount of reduction of total radiated sound power can also be obtained for on-resonance excitation cases. It is noted that design processes II and III generally perform better sound radiation control than design process I, because the PVDF sensor is not optimized in design process I. In theory, design process III optimizing the locations of PZT actuators and PVDF sensors simultaneously should provide the best optimum. However, as shown in Table VI, they are not always the cases. It is the cause that design process III involves more solution combinations and thus requires more population size in the GA to achieve the optimum. Since the GA discretizes the continuous solution domain, and even though sufficient resolution is provided, the optimal solution may not be exact. Nevertheless, the optimal solution is sufficient and satisfactory.

The control voltages required for PZT actuators are summarized in Table VII. One can see that lower frequency excitation cases require higher control voltages. All of the three design processes need about the same control efforts. In particular, for the first mode excitation the control voltages applied to the PZT actuators for design cases are about a half of that for the arbitrary case. For excitation at 80 Hz, i.e., between the first and second resonance, modes, the control voltages for design cases increases, because the lower

radiation modes required larger control effort in order to achieve sufficient sound radiation control.

To further study the control mechanisms of the optimized piezoceramic transducers, radiation directivity patterns and beam displacement distributions are plotted and compared as well as the wavenumber analysis. Figure 4 shows the radiation directivity patterns for various excitation frequencies. For 33 Hz excitation case, sound pressure level can be most significantly reduced to less than 0 dB because one actuator and one sensor are sufficient for controlling the first mode response. It is also interested to note that most of the residual radiation directivity patterns appear as dipole responses. This can be explained further in the following wavenumber analysis. In particular, for off-resonance excitation cases the optimum design cases can largely reduce sound pressure level about 25 dB for 80 Hz excitation case and 10 dB for 210 Hz excitation case. This agrees with the reduction of total radiated sound power as shown in Table VI.

Figure 5 shows the beam displacement distributions corresponding to the cases in Figure 4. It is noted that the PVDF sensor acts as a structural error sensor to reduce the slope difference between the edges of the PVDF film. The residual beam displacement is generally reformed to a higher modal response, as shown in Figures 5(a) and 5(c), which is a less efficient radiation mode [28]. It is interested to note that the beam displacement as shown in Figure 5(d) is in fact increased and reformed to the third modal response. This can also be evidenced by Table V which indicates that the third modal amplitude is increased by 5.7 dB, while the second modal amplitude is reduced by 6.6 dB. This means that the significant radiation modes are really reduced leading spillover to the less efficient radiation modes. Nevertheless, as shown in Figure 4(d) one can observe that the residual radiation directivity pattern is still like a dipole response, i.e., the second mode dominates the sound radiation.

As shown by Wang [14], through the wavenumber analysis the radiation mode shape appears in the directivity patterns exactly the same as the number of modes involved in the supersonic region. The LMS value of velocity transform plotted over the structural wavenumber (κ_x) is shown in Figure 6, when $\kappa_y = 0$, and the acoustic wavenumber ($\kappa = \omega/c$) is also indicated. As discussed previously, only those wavenumber components within supersonic region, i.e., $-\kappa < \kappa_x < \kappa$, contribute the sound radiation into the far field. In order to efficiently control the sound radiation, it is obvious to reduce the wavenumber components in the supersonic region. As one can see, the wavenumber components in supersonic region is largely reduced for all design cases. In particular, most of the wavenumber distributions appear a dip at $\kappa_x = 0$, and result in the dipole responses observed in Figure 4. It is also noted that for on-resonance excitation cases the wavenumber components are globally reduced, while for off-resonance case only those wavenumber components near the supersonic region are reduced and spillover occurs in the subsonic region. This again indicates that the efficient radiation modes are controlled leaving spillover to higher modes which are less efficient radiation modes.

CONCLUSIONS

This work presents the use of the GA incorporated with the LQOCT to optimally determine the locations of PZT actuators and PVDF sensors in active structural acoustic control. A simply-supported beam in an infinite rigid baffle subject to a harmonic point force is considered. Both finite length PZT actuators and PVDF sensors are used as control transducers in conjunction with the adoption of LMS feedforward control algorithm. The optimization problem is formulated, and a solution strategy based on the GA is proposed to determine the optimal locations of PZT actuators and PVDF sensors. Results show that the optimally positioned PZT actuators and PVDF sensors can perform better sound radiation control than the arbitrarily selected. The control mechanisms of piezoceramic transducers are also studied and compared in terms of radiation directivity patterns and beam displacement distributions as well as the wavenumber analysis. This works leads to an optimum design methodology for positioning actuators and sensors in active structural acoustic control.

ACKNOWLEDGEMENTS

The author gratefully acknowledges the support of the work by National Science Council, Republic of China, under grant NSC83-0401-E-020-008.

REFERENCES

1. Bailey, T., and J. E. Hubbard, "Distributed Piezoelectric-Polymer Active Vibration Control of a Cantilevered Beam," *Journal of Guidance Control*, Vol. 6, pp. 605-611 (1986).
2. Crawley, E. F., and J. de Luis, "Use of Piezoelectric Actuators as Elements of Intelligent Structures," *AIAA Journal*, Vol. 25, pp. 1373-1385 (1987).
3. Dimitriadis, E. K., C. R. Fuller, and C. A. Rogers, "Piezoelectric Actuators for Distributed Vibration Excitation of Thin Plate," *Journal of Vibration and Acoustics*, Vol. 113, pp. 100-107 (1991).
4. Wang, B. T., and C. A. Rogers, "Modeling of Finite-Length Spatially Distributed Induced Strain Actuators for Laminate Beams Structures," *Journal of Intelligent Material Systems and*

Structures, Vol. 2, pp. 38-58 (1991).

5. Wang, B. T., and C. A. Rogers, "Laminate Plate Theory for Spatially Distributed Induced Strain Actuators," *Journal of Composite Materials*, Vol. 25, pp. 433-452 (1991).
6. Clark, R. L., C. R. Fuller, and A. Wicks, "Characterization of Multiple Piezoelectric Actuators for Structural Excitation," *J. Acoust. So. Am.*, Vol. 90, pp. 346-357 (1991).
7. Clark, R. L., and C. R. Fuller, "Experiments on Active Control of Structurally Radiated Sound Using Multiple Piezoceramic Actuators," *J. Acoust. So. Am.*, Vol. 91, pp. 3313-3320 (1992).
8. Fuller, C. R., C. H. Hansen, and S. D. Snyder, "Experiments on the Active Control of Sound Radiation from a Panel Using a Piezoceramic Actuator," *Journal of Sound and Vibration*, Vol. 150, pp. 179-190 (1991).
9. Lee, C. K., and F. C. Moon, "Modal Sensors/Actuators," *Journal of Applied Mechanics*, Vol. 57, pp. 434-441 (1990).
10. Wang, B. T., C. R. Fuller, and E. K. Dimitriadis, "Active Control of Noise Transmission Through Rectangular Plates Using Multiple Piezoelectric or Point Force Actuators," *Journal of Acoustical Society of America*, Vol. 90, pp. 2820-2830 (1991).
11. Wang, B. T., C. R. Fuller, and E. K. Dimitriadis, "Active Control of Structurally Radiated Noise Using Multiple Piezoelectric Actuators," *AIAA Journal*, Vol. 29, pp. 1802-1809 (1991).
12. Wang, B. T., "The Performance of Accelerometers and PVDF Sensors in Active Structural Vibration Control," *Bulletin of National Pingtung Polytechnic Institute*, Vol. 3, pp. 81-92 (1994).
13. Clark, R. L., and C. R. Fuller, "Control of Sound Radiation with Adaptive Structures," *Journal of Intelligent Material Systems and Structures*, Vol. 2, pp. 431-452 (1991).
14. Wang, B. T., "Active Control of Far-Field Sound Radiation by a Beam with Piezoelectric Control Transducers: Physical System Analysis," *Smart Materials Structures*, accepted for publication (1994).
15. Chen, W. E., and J. H. Seifeld, "Optimal Location Process Measurements," *International Journal of Control*, Vol. 21, pp. 1003-1014 (1975).
16. Lindberg Jr., R. E. and R. W. Longman, "On the Number and Placement of Actuators for Independent Modal Space Control," *Journal of Guidance Control*, Vol. 7, pp. 215-221 (1984).
17. Martin, J. E., "Optimal Allocation of Actuators for Distributed Parameter Systems," *J. of Dynamic Systems, Meas. and Control*, Vol. 100, pp. 227-228 (1978).
18. Norris, G. A., and R. E. Skelton, "Selection of Dynamic Sensors and Actuators in the Control of Linear System," *J. Dynamic Systems, Meas. and Control*, Vol. 111, pp. 389-397 (1989).
19. Jia, J., "Optimization of Piezoelectric Actuator Design in Vibration Control Systems," Ph.D.Thesis, Department of Mechanical Engineering, Virgin Polytechnic Institute and State University, (1990).
20. Yang, S. M., and Y. J. Lee, "Optimization of Non-Collocated Sensor/Actuator Location and Feedback Gain in Control Systems," *Smart Materials Structures*, Vol. 2, pp. 96-102 (1993).
21. Wang, B. T., R. A. Burdisso, and C. R. Fuller, "Optimal Placement of Piezoelectric Actuators for Active Structural Acoustic Control," *Journal of Intelligent Material Systems and Structures*, Vol. 5, pp. 67-77 (1994).
22. Clark, R. L., and C. R. Fuller, "Optimal Placement of Piezoelectric Actuators and Polyvinylidene Fluoride Error Sensors in Active Structural Acoustic Control Approaches," *J. Acoust. So. Am.*, Vol. 92, pp. 1521-1533 (1992).
23. Goldberg, D.E., *Genetic Algorithms in Search, Optimization and Machine Learning*, Addison-Wesley, (1989).
24. Jenkins, W. M., "Structural Optimization with the Genetic Algorithm," *Struct.Eng.*, Vol. 69, pp. 418-422 (1991).
25. Riche, R. L., and R. T. Haftka, "Optimization of Laminate Stacking Sequence for Buckling Load Maximization by Genetic Algorithm," *AIAA Journal*, Vol. 31, pp. 951-956 (1993).
26. Holnicki-Szulc, J., F. Lopez-Almansa, and J. Rodellar, "Optimal Location of Actuators for Active Damping of Vibration," *AIAA Journal*, Vol. 31, pp. 1274-1279 (1994).
27. Wang, B. T., "Application of Genetic Algorithms to the Optimum Design of Active Control Systems," *Proceedings of International Noise and Vibration Control Conference*, pp. 231-236 (1994).
28. Wallace, C. E., "Radiation Resistance of a Baffled Beam," *J. Acoust. So. of Am.*, Vol. 51, pp. 936-945 (1972).
29. Fahy, F., *Sound and Structural Vibration*, Academic, Orlando, Florida, (1985).
30. Wang, B.T., *A Dynamic Simulation of Hybrid Active and Passive Control of Structural Vibration*, NSC Report: NSC81-0401-E-020-501, Republic of China, (1992).
31. Piezo Systems, Inc., *Product Catalog*, (1990).
32. Pennwalt Corporation, *Piezo Film Sensor Application Notes*, (1990).

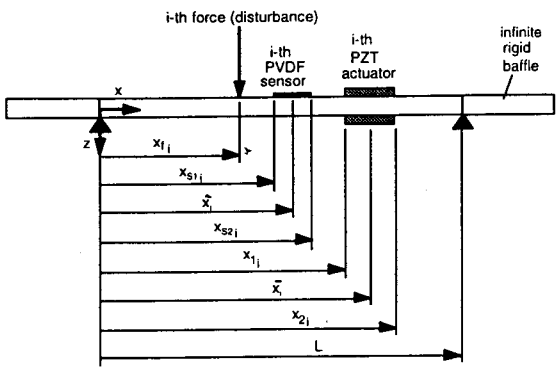

Figure 1. The arrangement and coordinates of simply supported beam

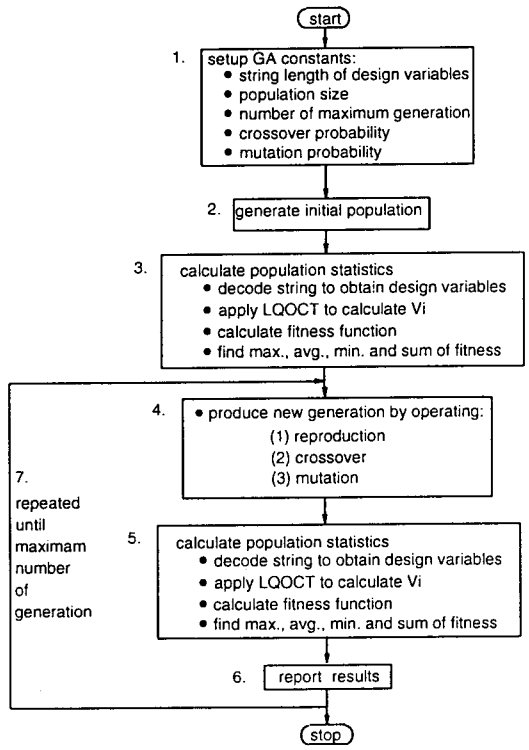

Figure 2. Flowchart of solution strategy

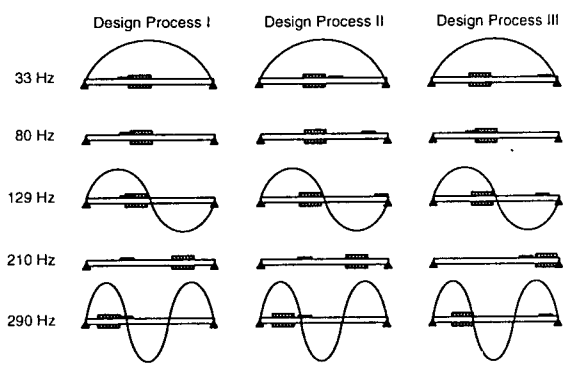

Figure 3. Optimal locations of PZT actuators and PVDF sensors

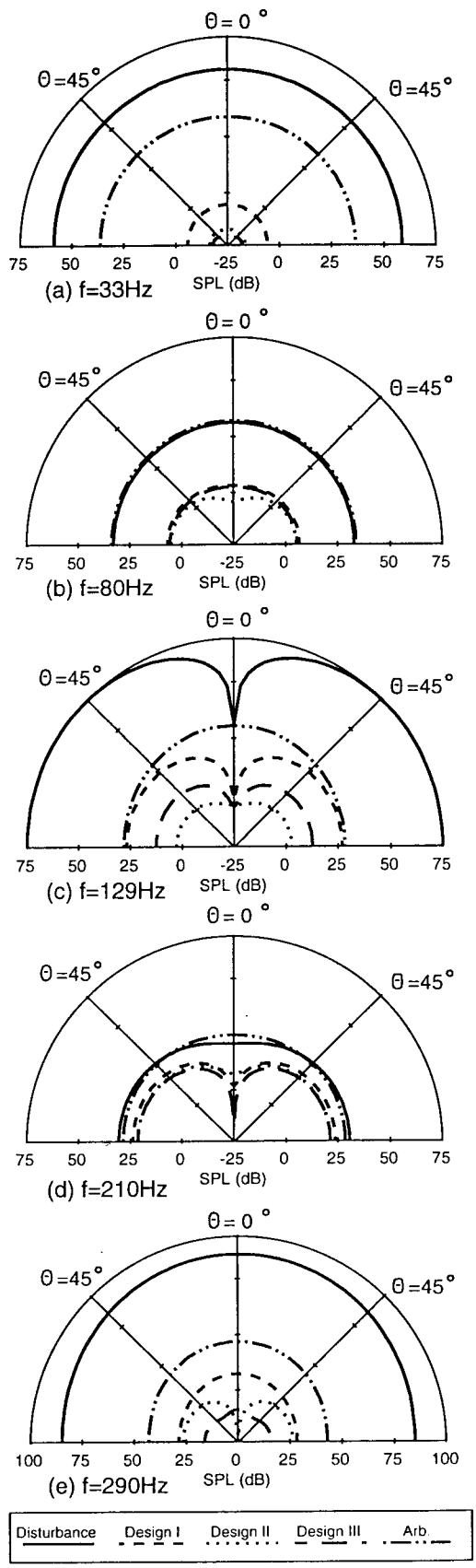

Figure 4. Radiation directivity pattern

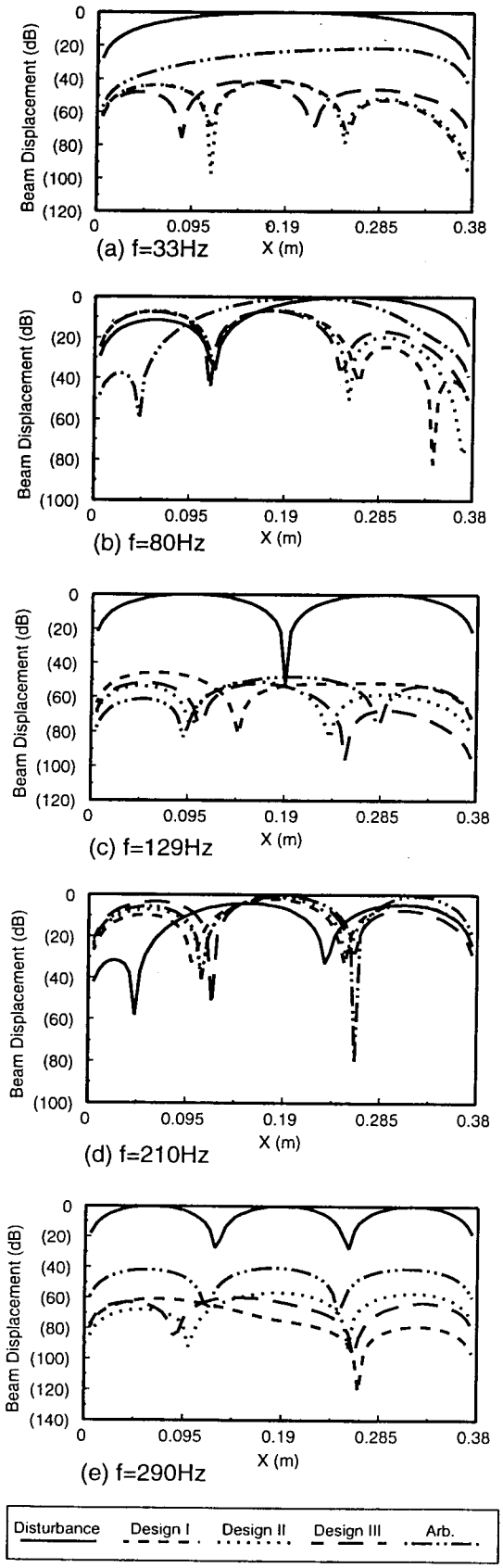

Figure 5. Beam displacement distributions

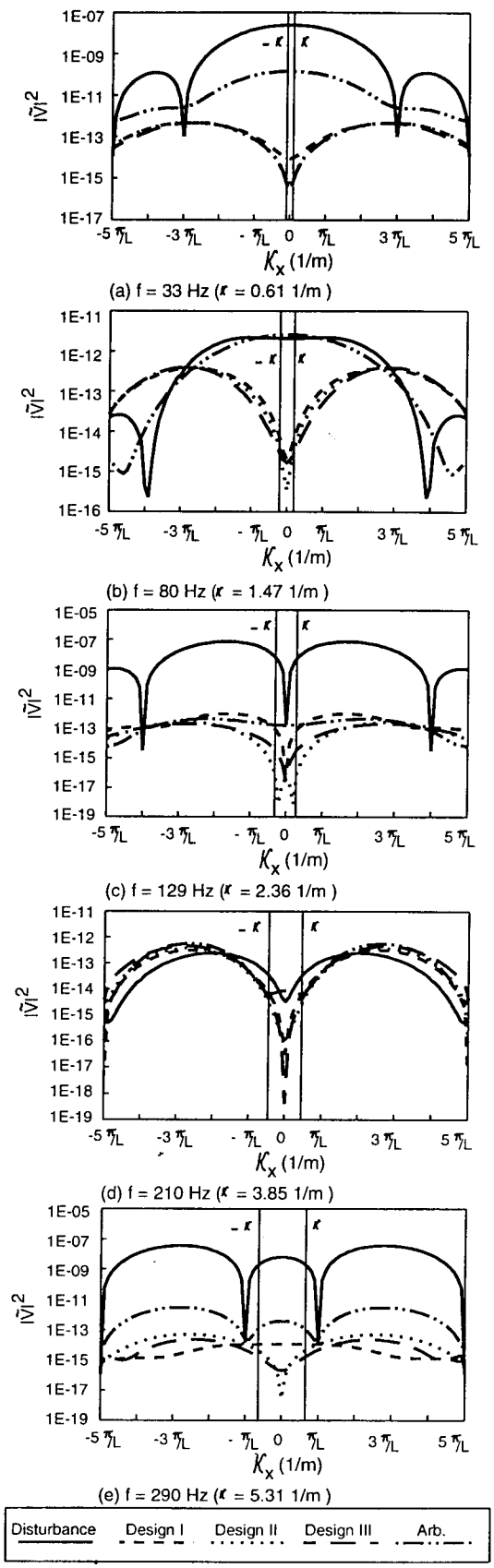

Figure 6. LMS values of velocity transform

Table I. Natural frequencies of the simply-supported beam

mode	frequency (Hz)
1	33.2
2	128.8
3	289.9
4	515.4
5	805.3
6	1159.6
7	1578.3
8	2061.4
9	2609.0
10	3220.9

Table II. Physical properties of the G-1195 piezoceramic patch [31]

$E_a = 6.3\times10^{10}(N/m^2)$	$\rho_a = 7650\ (Kg/m^3)$
$t_a = 1.905(mm)$	$\nu_a = 0.28$
$d_{31} = d_{32} = 166\times10^{-12}(\frac{m}{volt})$	

Table III. Physical properties of the PVDF films (LDT-28 μk) [32]

$E_s = 2\times10^{9}(N/m^2)$	$\rho_s = 1800\ (Kg/m^3)$
$t_s = 28\times10^{-6}(m)$	$\nu_s = 0.33$
$e_{31} = 54\times10^{-3}(C/m)$	$\epsilon = 106\times10^{-12}(F/m)$

Table IV. Optimal location of PZT actuators and PVDF sensors

excitation frequency (Hz)	Design (I) x_1, x_2	Design (II) x_{s1}, x_{s2}	Design (III) x_1, x_2	Design (III) x_{s1}, x_{s2}
33	**0.13396,0.19746**	**0.20772,0.24772**	**0.11447,0.17792**	**0.32105,0.36105**
80	0.13148,0.19498	0.30277,0.34277	0.12963,0.19313	0.09671,0.13671
129	**0.11570,0.17920**	**0.34000,0.38000**	**0.11478,0.17828**	**0.30909,0.34909**
210	0.25338,0.31688	0.10369,0.14369	0.24472,0.30822	0.21935,0.25935
290	**0.03805,0.10155**	**0.10967,0.14969**	**0.06002,0.12352**	**0.25923,0.29923**

Table V. Reduction of modal amplitude (dB) for Design Process I

f (Hz)	n=1	n=2	n=3	n=4	n=5
33	**52.8**	**20.3**	**-13.3**	**-17.4**	**-22.7**
80	14.5	14.4	-11.6	-16.5	-19.1
129	**8.9**	**49.6**	**-7.8**	**-16.8**	**-12.9**
210	-1.3	6.6	-4.7	0.1	-4.7
290	**2.1**	**5.7**	**73.8**	**5.6**	**4.4**

Table VI. Reduction of the total radiated power (dB)

f (Hz)	Design (I)	Design (II)	Design(III)	Arb.
33	**64.2**	**75.7**	**75.8**	**22.3**
80	29.1	33.1	29.8	-1.0
129	**48.3**	**71.0**	**62.4**	**39.1**
210	8.4	10.3	10.9	-0.9
290	**57.7**	**68.5**	**74.2**	**43.2**

Table VII. Control voltages of the PZT actuators (Volt)

f (Hz)	Design (I)	Design (II)	Design (III)	Arb.
33	**-52.54**	**-52.57**	**-55.16**	**-95.30**
80	-43.01	-44.97	-45.95	19.68
129	**-35.24**	**-35.10**	**-34.51**	**26.25**
210	12.10	15.83	26.24	16.73
290	**-12.08**	**-12.09**	**-15.67**	**-12.03**

壓電轉換器在主動結構噪音控制之最佳位置

王栢村

國立屏東技術學院
機械工程技術系

摘要

本篇論文在探討發展一套設計方法應用於主動結構噪音控制中壓電驅動器與感應器之最佳化位置設計。考慮在無限長剛體屏障之簡支樑受一簡諧激振點力作用，在最小平方前饋控制方式下，以壓電晶片黏貼於樑之表面作為控制驅動器，又以壓電薄膜作為結構型誤差感應器。架構以輻射聲能為基礎之目標函數，並定義壓電驅動器及感應器位置為設計參數之最佳化問題，配合線性平方最佳控制理論計算驅動器之控制電壓，以遺傳學演算法求得片狀壓電驅動器及感應器之最佳位置，結果顯示最佳化之壓電驅動器及感應器比任意選擇者，有較佳之聲音輻射控制，特別在非共振激振時，更可有效達到控制並減少散溢現象，輻射方向指向圖和樑之位移分佈分別用來驗證壓電轉換器之控制效果，並佐以波數場分析說明。